Journal of Applied Physics PERSPECTIVE scitation.org/journal/jap

# All-optical switch based on novel physics effects

Cite as: J. Appl. Phys. **129**, 210906 (2021); doi: 10.1063/5.0048878
Submitted: 27 February 2021 · Accepted: 8 May 2021 ·
Published Online: 4 June 2021



Huixin Qi,[1] Xiaoxiao Wang,[1] Xiaoyong Hu,[1,2,3,a)] Zhuochen Du,[1] Jiayu Yang,[1] Zixuan Yu,[1] Shaoqi Ding,[1] Saisai Chu,[1,a)] and Qihuang Gong[1,2,3]

## AFFILIATIONS

[1]State Key Laboratory for Mesoscopic Physics & Department of Physics, Collaborative Innovation Center of Quantum Matter & Frontiers Science Center for Nano-optoelectronics, Beijing Academy of Quantum Information Sciences, Peking University, Beijing 100871, People's Republic of China
[2]Peking University Yangtze Delta Institute of Optoelectronics, Nantong, Jiangsu 226010, China
[3]Collaborative Innovation Center of Extreme Optics, Shanxi University, Taiyuan, Shanxi 030006, China

[a)]**Authors to whom correspondence should be addressed:** xiaoyonghu@ pku.edu.cn and chusaisai@pku.edu.cn

## ABSTRACT

All-optical switches are among the most important parts of integrated photonics. Ultrahigh speed and ultralow energy consumption are two necessary indexes of all-optical switches. Traditionally, all-optical switches are based on concepts such as micro-ring resonators, surface plasmon polaritons, photonic crystals, and metamaterials. However, such platforms cannot satisfy the demand for high performance of all-optical switches. To overcome the limited response time and energy consumption, recent studies have introduced new applications of such physics as parity–time symmetry, exceptional points, topological insulators, and bound states in a continuum. Such physical concepts not only provide promising research avenues for the all-optical switch but also broaden the design channel. This is expected to achieve ultracompact, ultrafast, and high-capacity all-optical information processing.



## I. INTRODUCTION

The growth of global data has increased demand in information processing technology for ultralarge data transmission and ultrahigh information processing.[1] With the continuous development of fast electronic integrated circuits, researchers have considered using photons as information carriers to achieve ultrahigh speed and ultralow energy consumption with photon-integrated circuits.[2–4] All-optical switches are essential to integrated photonics because of their high on-chip performance, ultracompactness, high speed, and low power. An all-optical switch can be defined as a structure with a pump light controlling the ON/OFF transition of the signal light. An optical nonlinear material is an important part of the nanostructure whose change in refractive index depends on the intensity of the pump light, which mainly uses the third-order nonlinear optical Kerr effect.[5–7] Because of the ultrashort third-order nonlinear optical response to pump light and the large third-order nonlinear coefficient of the material, such switches can achieve a picosecond–femtosecond response time and lower energy consumption. The response time and energy consumption are the two main indexes of the optical switch.

Classical schemes for all-optical switches based on photonic crystals, surface plasmon polaritons (SPPs), micro-ring resonators, and metamaterials involve dynamical control of the cavity resonance via a pump pulse.[8] Traditional all-optical switches are mainly based on traditional physical structures. Over the last few decades, integrated optics have had significant progress in decreasing response time and energy consumption.[9–13] However, such structures cannot meet the requirements of high speed and high-capacity information processing. Researchers have introduced new physical structures based on these concepts to overcome such difficulties and realize all-optical switches. These structures have drawn much attention from the photonics community because they offer higher speed and larger capacity for information processing. In this review, we mainly introduce traditional concepts and methods of realizing an all-optical switch. Then, we detail the new physical applications of parity–time (PT) symmetry, exceptional points (EPs), topological insulators, and bound states in a continuum. Finally, we discuss the advantages of these applications over the traditional technology and speculate on their future development.

**TABLE I.** A comparison of the properties of the optical switching.

| Year | Switching principle structure | Pump intensity | Switching time | Q factor | ON/OFF contrast (dB) | Researchers |
|---|---|---|---|---|---|---|
| 2014 | Micro-ring resonator | 720 fJ/bit | 14.8 ps | $10^4$ | 23.3 | Pelc *et al.*[28] |
| 2014 | Micro-ring resonator | 25 mW | 25 ps | $10^4$ | >12.3 | Sethi *et al.*[41] |
| 2015 | Metamaterial | $10^1$–$10^2$ V/$\mu$m | … | … | >15 | Shaoei *et al.*[39] |
| 2017 | Photonic crystal | 560 kW/cm$^2$ | 15 ps | $10^4$ | 10 | Chai *et al.*[35] |
| 2018 | Surface plasmon polaritons | 1–10 MW/cm$^2$ | 1–2 ps | $10^1$ | 20 | Zhang *et al.*[31] |
| 2018 | Photonic crystal | $10^1$ mW/cm$^2$ | 1 ps | $10^1$ | 20 | Granpayeh *et al.*[42] |
| 2019 | Surface plasmon polaritons | 35 fJ/bit | 260 fs | … | 3.5 | Ono *et al.*[12] |
| 2019 | Photonic crystal | $10^2$ W/$\mu$m$^2$ | 15 ps | 1915 | 10 | Rebhi *et al.*[43] |
| 2020 | Metamaterial | 5 GW/cm$^2$ | 650 fs | $10^1$ | >15 | Xie *et al.*[40] |
| 2020 | Surface plasmon polaritons | 16.9 MW/cm$^2$ | … | $10^1$ | 21.93 | Khani *et al.*[44] |

## II. BASIC CONCEPTS AND DEVELOPMENT OF PERFORMANCE INDEXES

Traditional methods of realizing an all-optical switch rely on optical nonlinear effects and are mainly based on the shift in resonant wavelength. Researchers always consider reducing the response time and the pump power of the optical switch, so recently they have focused on effectively increasing the change in the refractive index. One way is to design the structure to increase the Q value of the resonator.[14,15] There are significant advantages to designing optical microcavities using micro-ring resonators, surface plasmon polaritons, photonic crystals, metamaterials, and other platforms with superior performance. The other is to find or produce materials with large third-order nonlinear coefficients. Examples of such materials are graphene[16–18] and ITO,[19–21] or designed multi-layer materials with improved nonlinear responses at specific wavelengths such as epsilon-near-zero (ENZ) wavelengths.[22,23] In this section, we mainly compare the properties of all-optical switches on the basis of traditional design and analyze the advantages and disadvantages of traditional design in terms of the performance of the all-optical switch itself. We summarize the development of all-optical switches in recent years in Table I, including the ON/OFF contrast, response time, pump intensity, and Q factor.

### A. Micro-ring resonators

Micro-ring resonators are among the most widely used configurations. The design of a micro-ring resonator is simple, its experimental preparation is easy, and at present its experimental conditions are relatively mature.[24,25] The principle of an all-optical ultrafast switch based on a micro-ring is to change the coupling between the waveguide and the micro-ring through a control light, which enables control of the signal light output. Switch control of the signal light output has been demonstrated using a nonlinear material and pump light to change the resonant frequency of the micro-ring, which is due to the refractive index variation of the nonlinear material. In 2007, Forst *et al.*[26] used two waveguides and a micro-ring covered with implanted $O^+$ ions to make an all-optical ultrafast switch with a reaction time of 55 ps, as shown in Fig. 1(a). In 2008, Waldow *et al.*[27] demonstrated a 25 ps all-optical switch based on a micro-ring, as shown in Fig. 1(b). The nonlinear

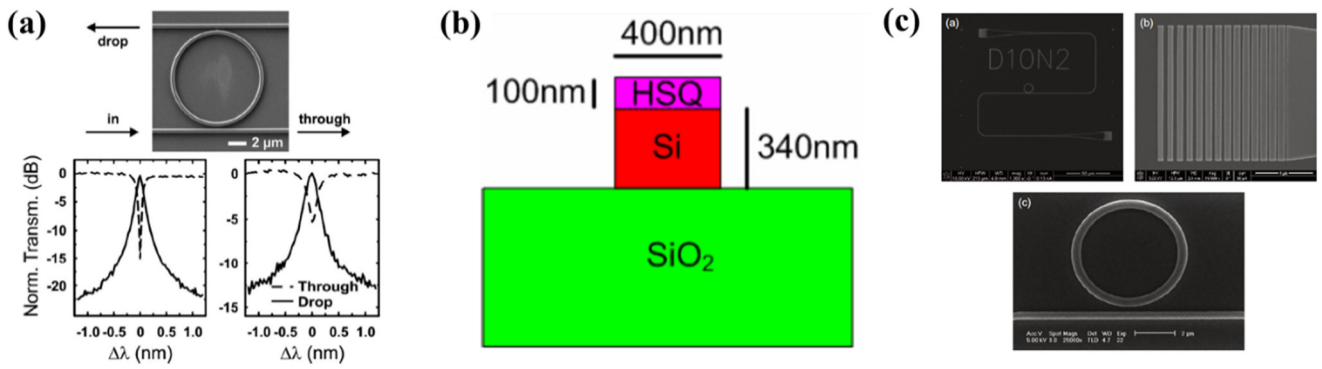


**FIG. 1.** Configuration characteristics of micro-ring devices. (a) Micrograph of the investigated micro-ring resonator after implantation.[26] Reproduced with permission from Wang *et al.*, Opt. Lett. **32**, 2046–2048 (2007). Copyright 2007, Optical Society of America. (b) Schematic cross-sectional view of the SOI waveguide.[27] Reproduced with permission from Waldow *et al.*, Opt. Express **16**, 7693–7702 (2008). Copyright 2008, Optical Society of America. (c) Scanning electron micrographs of a-Si: H devices after etching: layout of the micro-ring device with bus waveguide and grating couplers; close-up of the grating coupler for TM-polarized light; a 5-$\mu$m-diameter a-Si: H micro-ring and bus waveguide.[28] Reproduced with permission from Pelc *et al.*, Opt. Express **22**, 3797–3810 (2014). Copyright 2014, Optical Society of America.

material was hydrogen silsesquioxane (HSQ), which was used to cover the Si waveguide. In 2014, Pelc *et al.*[28] constructed an all-optical ultrafast switch with hydrogenated amorphous silicon micro-ring resonators, as shown in Fig. 1(c). They achieved a reaction time of up to 14.8 ps. The pulse width of the pump light was 2.7 ps, corresponding to a pulse energy of 3.0 pJ. They also measured the reaction time of a crystalline Si (c-Si) micro-ring resonator all-optical switch, which turned out to be 308 ps, 21 times longer than that of a switch based on an a-Si:H resonator. However, to obtain a microcavity with a high Q value, we need to increase the size of the micro-ring. Furthermore, the parameters for the optimal design of the micro-ring are relatively few. The advantages of the micro-ring resonator have been fully exploited, so it is necessary for researchers to find new configurations or introduce new physical ideas.

## B. Surface plasmon polaritons

Surface plasmon polaritons (SPPs) can greatly enhance a field with a very small footprint and have yielded excellent research results.[29,30] Attention has been given to SPP-based all-optical ultrafast switches in recent years. The basic idea is to control the propagation of the SPPs to change the optical path switch. One way to alter the propagation of the SPPs is using a pump light. In 2019, Ono *et al.*[12] constructed an all-optical ultrafast switch with a switching energy of only 35 fJ and a switching time that reached 260 fs, as shown in Fig. 2(a). They managed to couple the light from an Si waveguide into graphene-loaded deep-subwavelength plasmonic Au waveguides. This configuration promoted the absorption of the nonlinear material. In 2018, Zhang *et al.*[31] studied a tunable multichannel all-optical switch based on a plasmon-induced transparency (PIT) that worked at telecommunication wavelengths, as shown in Fig. 2(b). They covered the substrate with a silver layer and dug a metal–insulator–metal (MIM) plasmonic waveguide, a stub resonator, and square ring resonators (SRRs). The stub resonator was used to couple the waveguide and SRRs. They filled the SRRs with a nonlinear Kerr material or covered the SRRs with graphene layers. Both of these operations can help realize an all-optical switch. The switch worked at multiple wavelengths.

Lights with different polarizations transform differently in SPPs, which offers a potential method to realize an SPP-based all-optical switch. In 2020, Karabchevsky *et al.*[32] used light polarization to realize an SPP-based all-optical ultrafast switch, as shown in Fig. 2(c). Their all-optical sensor switch was realized by the excitation of molecular overtones in a hybrid plasmonic–dielectric configuration. Their switch was controlled by the polarization of the light, which was on when the incident light was a TM wave and off when it was a TE wave.

However, SPPs have not yet been applied to large-scale integrated devices because of their huge losses. The energy is usually almost completely lost within a few micrometers of the propagation distance, resulting in the formation of SPP modes that cannot be transmitted normally in the device structure. Therefore, research on SPPs is also currently limited to a single device or several devices.

## C. Photonic crystals

Photonic crystals (PCs) have fairly good wavelength selectivity. The mode volume of a photonic crystal microcavity is very small, which provides an excellent platform for a photonic integrated circuit.[33,34] However, the transmission spectrum changes when the pump light is injected into the system. For injected light at some wavelengths, the propagation state changes from allowed to forbidden or from forbidden to allowed, making it possible to make an all-optical switch. In 2016, Colman *et al.*[8] demonstrated a nanocavity-based photonic crystal all-optical switch, as shown in Fig. 3(a). They dug an input waveguide, an output waveguide, and a nanocavity in the photonic crystal. They found that the resonance wavelength of the cavity could be changed by either the Kerr effect or free carriers, but the latter was better. Furthermore, they proved the importance of coherent effects, which are always ignored when studying nanocavity dynamics. In 2017, Chai *et al.*[35] demonstrated an ENZ nanocomposite-based ultrafast all-optical switch that could be triggered remotely, as shown in Fig. 3(b). They dug two nanocavities and three silicon photonic crystal waveguides, two of which were used to couple the nanocavities to the signal transmission waveguide. The resonance wavelength of the nanocavity was near 1560 nm. However, coupling the two nanocavities with each other caused Rabi splitting of the resonance

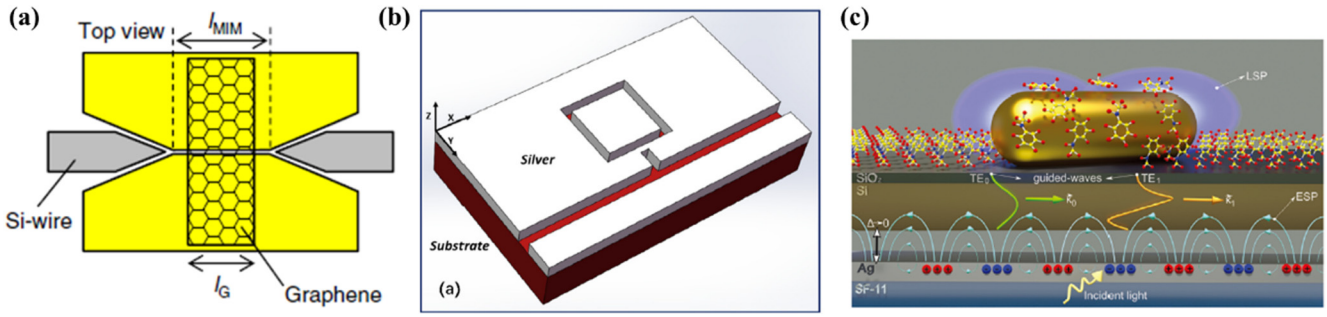


**FIG. 2.** Configuration characteristics of SPP devices. (a) Top-view schematic of the graphene-loaded MIM-WG.[12] Reproduced with permission from Ono *et al.*, Nat. Photonics **14**, 37 (2020). Copyright 2020, Springer Nature. (b) 3D schematic of structure with multilayer graphene. The relevant structure parameters: $w = 100$ nm, $s = 123$ nm, $h = 190$ nm, $g = 15$ nm, $w' = 50$ nm, and $L = 405$ nm.[31] Reproduced with permission from Zhang *et al.*, Opt. Commun. **425**, 196–203(2018). Copyright 2018, Elsevier BV. (c) The coupling mechanism of the hybrid GWSPR-LSPR-overtone system (out of scale, the gap between the Ag and the Si layers is infinitesimally small with $\Delta \to 0$).[32] Reproduced with permission from Karabchevsky *et al.*, Adv. Opt. Mater. **8**, 2000769 (2020). Copyright 2020, Wiley-VCH Verlag GmbH & Co. KGaA, Weinheim.

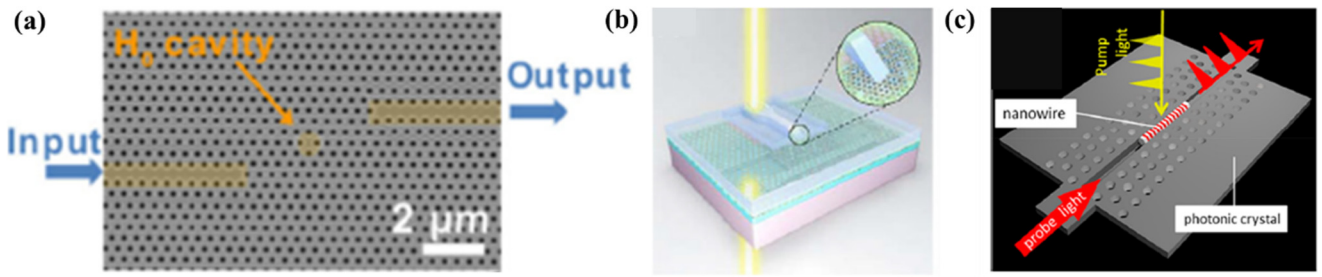


**FIG. 3.** Configuration characteristics of photonic crystal devices. (a) SEM image of the $H_0$ cavity and its access waveguides.[8] Reprinted with permission from Colman, Phys. Rev. Lett. **117**, 233901 (2016). Copyright 2016 American Physical Society. (b) Structure schematic and scanning electron microscope (SEM) image of the remotely coupled photonic crystal nanocavities sample without the monolayer graphene, the nanocomposite nano-Au:($Er^{3+}$:$Al_2O_3$) layer, and the uppermost $Er^{3+}$:$Al_2O_3$ waveguide. A and B indicate the photonic crystal nanocavities. I and O indicate the input- and output-coupling ports for the bus signal waveguide.[35] Reproduced with permission from Chai *et al.*, Laser Photonics Rev. **11**, 1700042 (2017). Copyright 2017, Wiley-VCH Verlag GmbH & Co. (c) Schematic representation of a single-nanowire all-optical switch on a silicon PC.[36] Reproduced with permission from Takiguchi *et al.*, ACS Photonics **7**, 1016 (2020). Copyright 2020, American Chemical Society.

wavelength. Light at the wavelengths of 1559.8 and 1560.2 nm was forbidden, while light at the wavelengths of 1560 nm could propagate. To activate the switch, pump light with an intensity of 560 $kW/cm^2$ was injected into nanocavity A, causing its resonant wavelength to increase slightly. The effect was that the coupling between the nanocavities was greatly weakened, the Rabi splitting disappeared, and light at the wavelength of 1560 nm was forbidden. This all-optical switch had a response time of up to 15 ps.

In 2020, Takiguchi *et al.*[36] first demonstrated a picosecond all-optical switch using a nanowire, as shown in Fig. 3(c). They put an InP/InAsP nanowire on a silicon photonic crystal. The line-defect photonic crystal had a Q-factor of 25,000. Then, they found that the λ_pr-λ_c detuning was −0.25 nm, which contributed to the fastest reaction (λ_pr represents the probe laser wavelength while λ_c is the cavity wavelength). The reaction time of the switch was 150 ps, while the switching energy was several hundred fJ. The switch time and energy were both lower than the previously reported results.

However, the design parameters of the photonic crystal structure are also limited. Recently, researchers have introduced topology into the platform of a photonic crystal and discovered new physical phenomena.

### D. Metamaterials

Metamaterials are artificial microstructures arranged according to certain rules at the subwavelength scale that achieve an

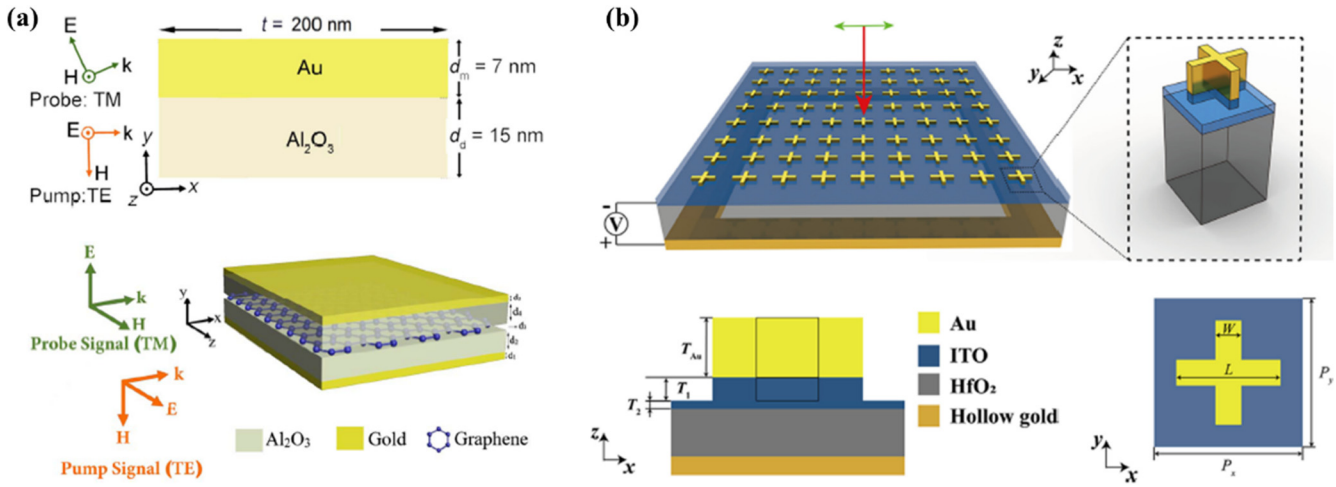


**FIG. 4.** Configuration characteristics of metamaterial devices. (a) Side (x–y plane) view of the unit cell of the HMM structure, composed of $Au/Al_2O_3$ nanolayers, under the illumination of a TE-polarized Gaussian pump and a TM-polarized CW probe. Unit cell of a switchable HMM, composed of $Au/Al_2O_3/G/Al_2O_3/Au$ nanolayers, periodically repeated in the y-direction. Inset on the left depicts a TE-polarized pump signal and a TM-polarized probe signal.[39] Reproduced with permission from Shoaei *et al.*, J. Opt. Soc. Am. B **32**, 2358–2365 (2015). Copyright 2015, Optical Society of America. (b) 3D schematic overview of the proposed structure, with a cross-shaped array of Au and ITO located on top of an ITO nanofilm on the $HfO_2$ substrate. An x-polarized plane wave normally incident on the metasurface.[40] Reproduced with permission from Xie *et al.*, IEEE Photonics J. **12**, 4501510 (2020). Copyright 2020, IEEE Photonics Society.

arbitrary equivalent dielectric constant and permeability.[37] Metamaterials can be electromagnetically controlled more than natural materials, and their unique electromagnetic response mainly comes from the structural design.[38] In 2020, Shoaei *et al.*[39] used nonlinear hyperbolic metamaterials to design an all-optical switch that worked in the visible and near-infrared regions, as shown in Fig. 4(a). They investigated three kinds of metamaterials. The first consisted of Au–$Al_2O_3$ nanolayers. A switch with this nanolayer was realized in the 585–600 nm range, and the transmittance of the "ON" state was 52%–72%. They used a 500 V/$\mu$m pump signal. The second consisted of Au/$Al_2O_3$/G (graphene)/$Al_2O_3$/Au nanolayers and had a work range of 803–805 nm, a transmittance reaching 97%, and a 4 V/$\mu$m pump signal. The last consisted of Ag/Si/G/Si/Ag nanolayers and could work over a wider wavelength range, 800–895 nm. The transmittance of the "ON" state was 49%–99%, and the pump signal they used was 19.5 V/$\mu$m. In 2020, Xie *et al.*[40] designed an ENZ metasurface-based optical switch that could be controlled electronically or optically, as shown in Fig. 4(b). When it was used as an all-optical switch, the pump light was incident on the metasurface with an angle (θ), inducing the nonlinear response of the ITO material at the ENZ wavelength (1240 nm). The transmission of the probe light could be tuned using both θ and the pump light intensity. The extinction ratio was over 5 dB, and the reaction time was about 650 fs.

A metamaterial is an excellent platform for optical signal processing, but it is not suitable for on-chip optical signal processing. Future research can consider the implementation of on-chip optical signal processing on a metamaterial platform.

## III. NEW PHYSICAL EFFECTS TO REALIZE AN ALL-OPTICAL SWITCH

Compared with the traditional design methods, introducing new physical effects to the all-optical switch can overcome the bottleneck of the response time and the energy consumption and achieve superior performance. For example, broadband allows a very wide range of wavelengths. Other performance features such as high contrast and high robustness can be realized by introducing topology to avoid device error during preparation. New signal and control degrees are also added when using these physical concepts. For example, the all-optical switch is realized via mode conversion or polarization conversion in a non-Hermitian system by encircling an EP and controlling the gain or loss of the system. It is possible to make an all-optical switch with high robustness and high contrast by transforming the body state and boundary state in the topological system. We can construct a continuous bound state to make an all-optical switch with an infinite Q value, breaking through the limited Q value of the traditional structure. As another example, a wideband all-optical switch with low energy consumption can be constructed using the saturable absorption of a new 2D material. In Sec. III, we introduce four physical principles that can be used to realize an all-optical switch. We analyze their advantages and provide some suggestions for future development.

### A. PT symmetry and exceptional points in an all-optical switch

#### 1. Non-Hermitian systems and PT symmetry in optics

The concepts of a non-Hermitian system and PT symmetry first arose in quantum field theory. For a physical system described by a Hamiltonian $\hat{H}$, the equation $\hat{H} = \hat{H}^{\dagger}$ means the system is Hermitian with real energy eigenvalues and complete orthonormal eigenstates. However, if the Hamiltonian is not invariant under a Hermitian conjugate, the system is non-Hermitian. In general, a non-Hermitian system has open boundary conditions or just has gain or loss. A non-Hermitian system can have imaginary energy eigenvalues unless the system has PT symmetry.[45] Consider a non-Hermitian Hamiltonian $\hat{H} = \frac{\hat{p}^2}{2m}$. If $\hat{H}$ has PT symmetry, which means $[\hat{H}, \hat{P}\hat{T}] = 0$, the complex potential must satisfy $V(x) = V(-x)^*$.

The concepts of the non-Hermitian system and PT symmetry are also widely used for optical systems. First, we start with the paraxial wave equation of diffraction in optics,

$$i\frac{\partial \vec{E}(x,z)}{\partial z} + \frac{1}{2k}\frac{\partial^2 \vec{E}(x,z)}{\partial x^2} + k_0 \tilde{n}(x)\vec{E}(x,z) = 0, \tag{1}$$

where $\tilde{n}(x)$ is the complex refractive index distribution.[46–48] This equation is mathematically isomorphic to the Schrödinger equation, so we can establish the equivalence between quantum theory and light dynamics. Therefore, the effective Hamiltonian of the paraxial wave equation can be expressed as

$$\hat{H} = -\frac{1}{2k}\frac{\partial^2}{\partial x^2} - k_0 \tilde{n}(x). \tag{2}$$

For a non-Hermitian PT-symmetric optical system, the complex refractive index distribution should satisfy $\tilde{n}(x) = \tilde{n}(-x)^*$.

An easier way to build a PT-symmetric optical system is to use the following coupled mode equations:[49]

$$\frac{d}{d\xi}\begin{pmatrix} a_1 \\ a_2 \end{pmatrix} = -i\begin{pmatrix} \omega_1 - i\gamma_1 & \kappa \\ \kappa & \omega_2 - i\gamma_2 \end{pmatrix}\begin{pmatrix} a_1 \\ a_2 \end{pmatrix}. \tag{3}$$

According to the coupled mode equations, all we need to establish a PT-symmetric system are two coupled optical systems or just two coupled modes whose parameters satisfy particular conditions to make the eigenvalues real. We can freely use two coupled waveguides, two coupled cavities, or generally several waveguides and several resonators coupled with each other.

As an example, two coupled waveguides can form a PT-symmetric system with gain and loss.[50,51] As shown in Fig. 5, two waveguides with constant coupling strength are fabricated from Fe-doped $LiNbO_3$. The gain in this system is built up through two-wave mixing by selectively irradiating one of the waveguides with a pulsed laser. The other waveguide has a loss, which is from the optical excitation of electrons from $Fe^{2+}$ centers to the conduction band.

Another kind of system does not have PT symmetry, such as a system that only has loss without gain. Nevertheless, gauge transformation can reveal the hidden PT symmetry and transfer the

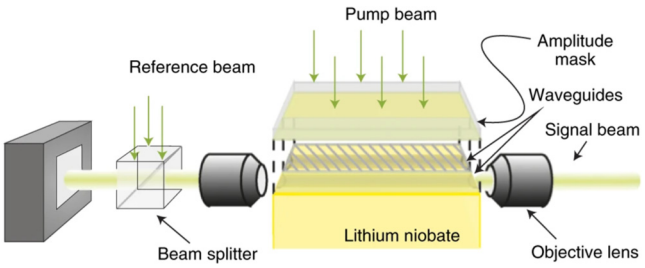


**FIG. 5.** A PT-symmetric system consisting of two coupled waveguides: An $Ar^+$ laser beam (wavelength 514.5 nm) is coupled into the arms of the structure. An amplitude mask blocks the pump beam from getting into channel 2, enabling two-wave mixing gain only in channel 1.[50] Reproduced with permission from Ono *et al.*, Nat. Photonics **14**, 37 (2020). Copyright 2020, Springer Nature.

Hamiltonian to the one with PT symmetry. The properties of the PT symmetry remain in this kind of system, which is called a passive PT symmetric system.[52]

### 2. Fundamentals of exceptional points

In a non-Hermitian PT symmetric system, there can be EPs where the eigenvalue degenerates as well as the eigenstates. EPs are also called non-Hermitian exceptional points because they are quite different from the degenerate points (Dirac points) (DPs) in a Hermitian system. At DPs, the eigenvalue degenerates but the eigenstates are non-degenerate. However, at EPs, the eigenstates also degenerate, which means the eigenspace at an EP has a lower dimension.

Take a two-dimensional set of coupled mode equations as an example. The effective Hamiltonian can be expressed as

$$\begin{pmatrix} \omega_1 - i\gamma_1 & \kappa \\ \kappa & \omega_2 - i\gamma_2 \end{pmatrix}. \tag{4}$$

We can derive the eigenvalues according to the Hamiltonian

$$\sigma_{\pm} = \omega_{ave} - i\gamma_{ave} \pm \sqrt{\kappa^2 + (\omega_{diff} + i\gamma_{diff})^2}, \tag{5}$$

where $\omega_{ave} = (\omega_1 + \omega_2)/2$ and $\gamma_{ave} = (\gamma_1 + \gamma_2)/2$ represent the mean values of the frequencies and loss factors of the two subsystems, $\omega_{diff} = (\omega_1 - \omega_2)/2$ and $\gamma_{diff} = (\gamma_1 - \gamma_2)/2$ are the differences between their frequencies and loss factors, and $\kappa$ is the coupling strength. If we assume $\kappa$, $\omega_{ave}$, and $\gamma_{ave}$ are constant, we evaluate the evolution of the real and imaginary parts of the eigenvalues in the parameter space ($\omega_{diff}$, $\gamma_{diff}$), as shown in Figs. 6(a) and 6(b).[49] We know that for a PT-symmetric system, the imaginary part of each eigenvalue vanishes, so $\omega_{diff} = 0$, $\gamma_{ave} = 0$, and $\gamma_{diff} < \kappa$. The EP is at (0, $\kappa$) in Figs. 6(a) and 6(b), and the parameters allowing PT symmetry are on one side of the EP.

If we change the coupling strength $\kappa$, the eigenvalues evolve,[51] as shown in Figs. 6(c) and 6(d). We can approach the EPs or break PT symmetry by controlling the parameters of the system. Clearly, EPs are the critical points when breaking the PT symmetry.

### 3. Exceptional points applied to an all-optical switch

EPs in an optical system have attracted much attention in recent years. Research on EPs is focused on encircling EPs and enhancement effects around EPs. Encircling EPs is a remarkable method for an all-optical switch.

Theoretically, when two parameters of the system are controlled and others remain constant, the eigenvalue will evolve along a particular path on the Riemann surface in the parameter space, like ($\omega_{diff}$, $\gamma_{diff}$) in Figs. 6(a) and 6(b). When the parameters are changed sufficiently slowly and an EP is continuously encircled, an adiabatic state begins to evolve. As shown in Figs. 7(a) and 7(b), the end point of the path and the mode switches are possibly on different Riemann sheets while the EP is encircled. Which Riemann sheet the end point will be on only depends on whether the loop is clockwise (CW) or counterclockwise (CCW).[53]

For example, in 2016, Doppler *et al.* applied the theory of EP encirclement to a two-mode waveguide and proved the theory experimentally.[53] The eigenstates of the effective Hamiltonian are the even and odd modes in this waveguide. The two parameters, the coupling $g$ and detuning $\delta$, are controlled through smooth variation of the modulation potential of the waveguide. As shown in Fig. 7(c), the EP is encircled when propagating through the designed waveguide, and only one of the two transverse modes gets through the waveguide depending on the injection direction. Right and left injection corresponds to the CW and CCW loop, respectively.

Similarly, in 2017, Hassan *et al.* theoretically proved EP encirclement by solving the differential equation mathematically.[54] They re-casted the coupled mode equations as a second-order differential equation whereby two parameters encircle the EP and depend on only one parameter. This can be reduced to a degenerate hypergeometric differential equation. Then, by showing asymptotic expansion when the EP is encircled slowly enough, they proved the mode switch after the encirclement. They applied the theory to the right-trapezoidal waveguide in Fig. 8(a) and to the eigenstates. Varying the width and pumping of the waveguide can achieve the EP encirclement in Fig. 8(b). No matter what polarization state is injected into the waveguide, the output will only be one of the eigenstates in Fig. 8(a) depending on whether the design of this waveguide produces the CW or the CCW loop.

Second-order EPs have two degenerate eigenvalues and eigenmodes and are now widely used to achieve all-optical switches. Higher-order EPs have also been used.[55] There are different ways to design an optical system, each with its own way to approach and encircle the EPs and achieve a mode switch. EPs have received more and more attention in recent years.

## B. Topological insulators in an all-optical switch

### 1. Introduction of topological insulators

The initial idea of topological insulators arose from condensed matter physics, particularly electrons moving along the surfaces of specially designed materials. In brief, topological insulators are materials that behave as insulators in their interior but are conductive on their surfaces.[56]

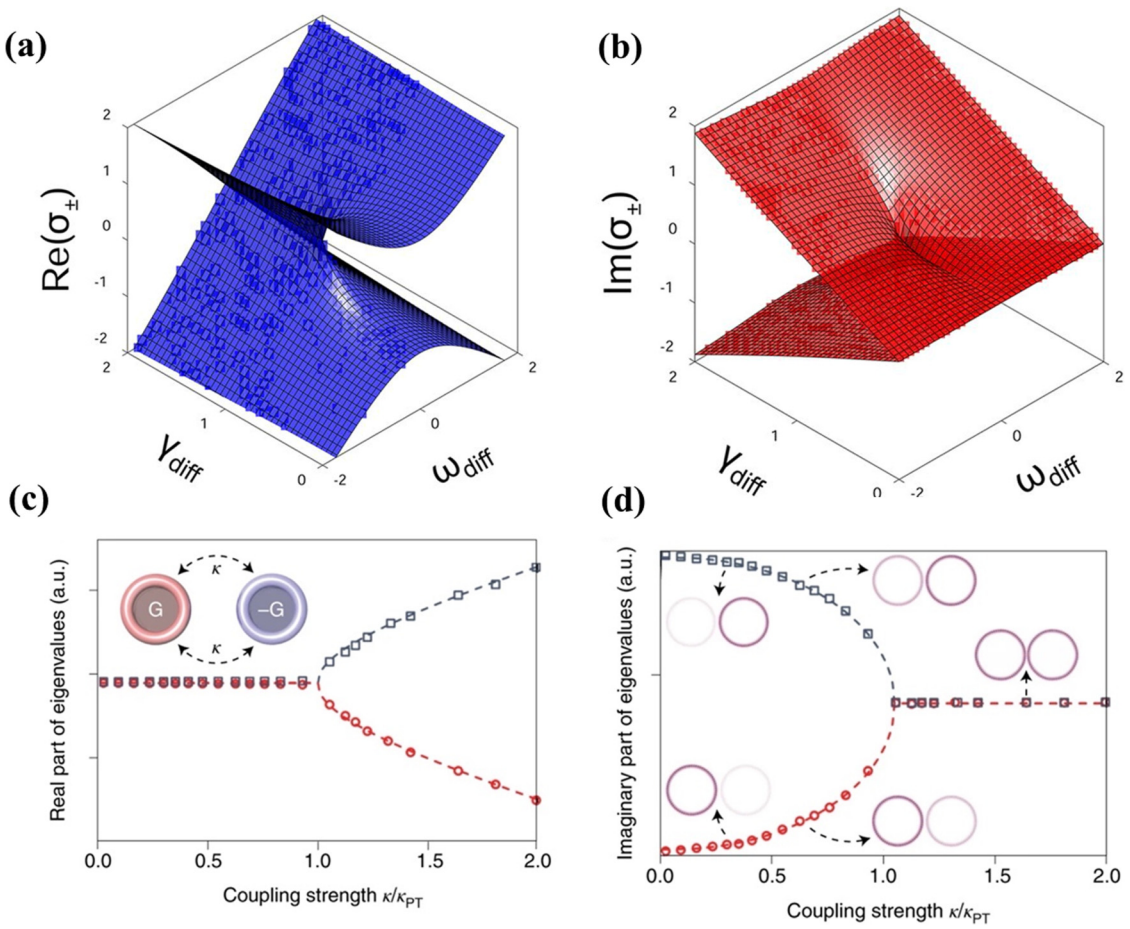


**FIG. 6.** Evolution of eigenvalues while changing parameters of the system. [(a) and (b)] Evolution of the real (a) and imaginary (b) parts of the eigenvalues of the system described by two-dimensional coupled mode equations in the two-dimensional parameter space ($\omega_{diff}$, $\gamma_{diff}$). Each diagram is a Reimann surface with two sheets.[49] Reproduced with permission from Miri and Alu, Science **363**, 42 (2019). Copyright 2019, Optical Society of America. [(c) and (d)] Evolution of the real (c) and imaginary (d) parts of the eigenvalues of the system when changing the coupling strength $\kappa$. Red circles and blue squares are obtained by numerical simulation in COMSOL assuming that the system is composed of resonators. $\kappa$ is normalized to the critical coupling strength $\kappa_{PT}$ at which the system approaches the EP.[51] Reproduced with permission from Ozdemir *et al.*, Nat. Mater. **18**, 783 (2019). Copyright 2019, Springer Nature.

Topological insulators are well studied because of their useful properties and promising applications. The most well-known property of traditional topological insulators is allowing electrons to propagate along the boundary, neglecting defects, and not dissipating even if there are corners or turns. Photonic topological insulators can be used to design low-loss waveguides. A non-trivial topological insulator also allows a gas of helical Dirac fermions that behave like massless relativistic fermions. Furthermore, topological insulators exhibit spin-momentum locking, which can be used to design spintronic devices.

Photonic topological insulators are just like topological insulators, but the relevant particles are photons rather than electrons. The theories of photonic topological insulators are mostly the same as those of electronic topological insulators. They can provide robust unidirectional channels for light propagation, as expected.

The special properties of topological insulators are quite promising and give them advantages over traditional designs in the aforementioned applications. There are various models of topological insulators owing to the different ways to fulfill topological properties.

### 2. Application of topological insulators in an all-optical switch

Valley photonic crystals, for example, can be used to realize topological optical switches and have some important advantages. In 2018, Wu *et al.*[57] theoretically proposed a design for a topological optical switch while studying reconfigurable topological states in valley photonic crystals, as shown in Fig. 9. They simply constructed two topologically distinct valley photonic crystals to form

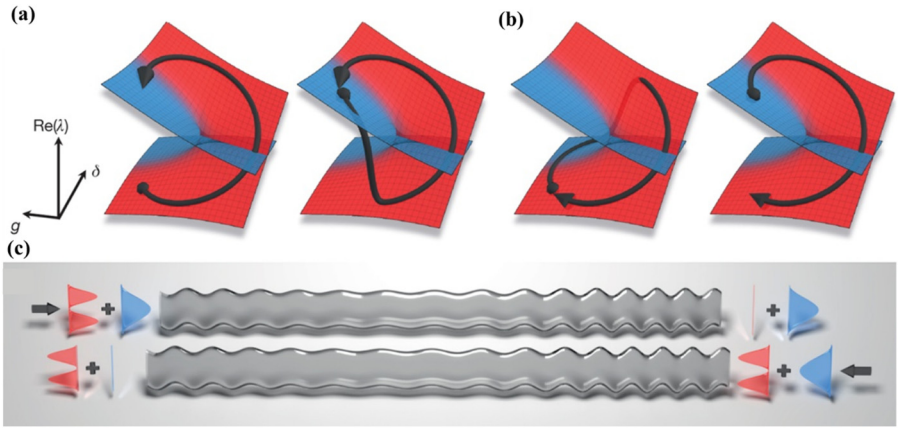


**FIG. 7.** Mode switch when encircling EP. [(a) and (b)] Encircling EP counterclockwise (a) or clockwise (b), then the end point will always be on the blue (a) or red (b) Reimann sheet, which means transfer to an odd mode or even mode, respectively. (c) Two-mode waveguide designed to perform an EP-encircling while propagating through it. Injection from the right or left accomplishes the EP-encircling clockwise or counterclockwise, respectively.[53] Reprinted with permission from Doppler *et al.*, Nature **537**, 76 (2016). Copyright 2016 Springer Nature.

a two-port optical switch. The inversion symmetry was broken by tuning the refractive index of one rod in each unit cell, leading to nontrivial topology locked to each valley. The working frequency was $\omega = 0.3678a/2\pi c$, where $D > 92\%$ for both ports. The ON/OFF ratio was 32.8 (28.9) for the left (right) port. This two-port optical switch not only performed well but also tolerated some defects or impurities owing to the topological protection.

The low-dimensional topological insulator $Bi_2Se_3$ has a quantum phase characterized by an insulating bulk bandgap and metallic surface states. Figure 10 shows a hybrid nanoantenna constructed with the topological insulator $Bi_2Se_3$–Au. In 2019, Miao *et al.*[58] used the polarization-sensitive non-linear absorption of this nanoantenna to design an optical switch that was easily modulated by simply rotating the light polarization with a right angle. The polarization-sensitive non-linear absorption came from the localized surface plasmon resonance of $Bi_2Se_3$–Au. The advantage of this design is that it can be used in purely optical systems without introducing complex structures. It can also be easily manipulated. Through a light-control system, a transmittance intensity of continuous-wave probe light with a wavelength of 450 and 1064 nm was modulated with 800 nm fs-laser pump light ($\sim$10 GW cm$^{-2}$).

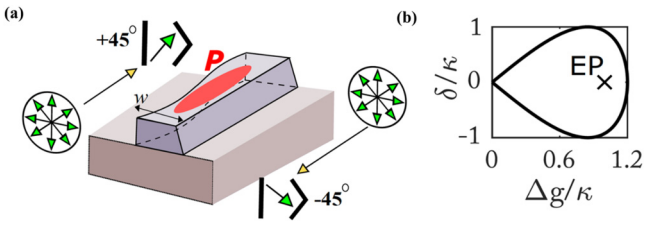


**FIG. 8.** The designed waveguide to achieve polarization modes switch: (a) The waveguide with variations in the width (w) sinusoidally and pumping (*P*), which is strongest in the center. The eigenstate of the system is shown by green arrowheads. (b) EP-encircling in the parameters space for this system. Detuning is given by $\delta$ and $\Delta g$ represents the difference between the TE and TM modal gains.[54] Reprinted with permission from Hassan *et al.*, Phys. Rev. Lett. **118**, 093002 (2017). Copyright 2017 American Physical Society.

Thus, the "ON" and "OFF" modes were induced by the intensity of the probe light with this structure-based switch.

In 2020, Lin *et al.*[59] presented tunable light absorption of graphene using topological interface states. The monolayer graphene was embedded in the interface of asymmetric topological photonic crystals, as shown in Fig. 11. Topological interface states excite strong absorption whose intensity is strongly related to the chemical potential of graphene and the periodic number of the asymmetric topological photonic crystals. As a result, the absorption near 1.2 eV was quickly attenuated in a tiny region as long as the chemical potential slightly varied. This benefits application to optical switches and other devices.

## C. Bound states in the continuum of an all-optical switch

### 1. Bound states in a continuum

Bound states in a continuum (BICs) are waves that are spatially localized where they coexist with continuous radiation waves that carry energy away. This is a general wave phenomenon observed in photonics, acoustics, and elastic waves that was originally proposed by von Neumann and Wigner for custom-constructed potentials in an electronic system.

In an open system, the frequency spectrum generally consists of a continuous spectrum of one or more extended states capable of propagating energy outward and several discrete bound states resulting from multiple potential wells. There are several different mode profiles. The mode profile in discrete levels of conventional bound states (green line in Fig. 12) is the regular bound state confined to a structure or potential (black dashed line in Fig. 12).[60] It has no channel to carry an outgoing flux and couple with the outer environment because it does not have enough energy to escape the confinement well. The ordinary mode profiles that exist across a continuous range of frequencies are extended states (blue line in Fig. 12) that can propagate energy outward. A leaky mode appears in the continuum that is capable of coupling to the extended waves and leaks out. This resonance (orange line in Fig. 12) can be expressed with a complex frequency, $\omega = \omega_0 - i\gamma$, where $\omega_0$ is the resonance frequency and $\gamma$ is the leakage rate. The BIC (red line in

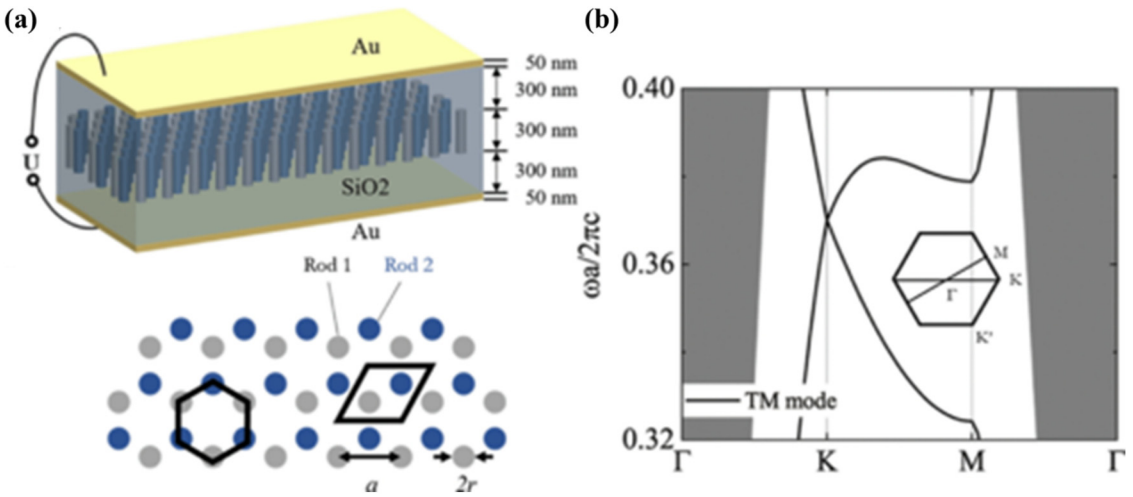


**FIG. 9.** (a) Three-dimensional configuration of the reconfigurable valley photonic crystal. The photonic crystal rod slab is embedded in an $SiO_2$ layer and covered by two gold films. The band structure of the TM mode for the two-dimensional photonic crystals when $n_{TiO2} = n_{BTO}$. (b) Schematic representation of a two-dimensional model of the valley photonic crystal composed of $TiO_2$ (rod 1, gray rods) and $BaTiO_3$ (rod 2, blue rods).[57] Reprinted with permission from Wu *et al.*, Phys. Rev. Mater. **2**, 122201 (2018). Copyright 2018 American Physical Society.

Fig. 12) is an exception to the conventional cases mentioned above. Although it resides within the spectral continuum of propagating waves that radiate to the far field, the BIC decouples completely from the extended waves, so it remains perfectly confined without any radiation. A BIC is always considered a resonance without leakage ($\gamma = 0$); in other words, a BIC has a zero linewidth and an infinite quality factor ($Q = \omega_0/2\gamma$).[61,62]

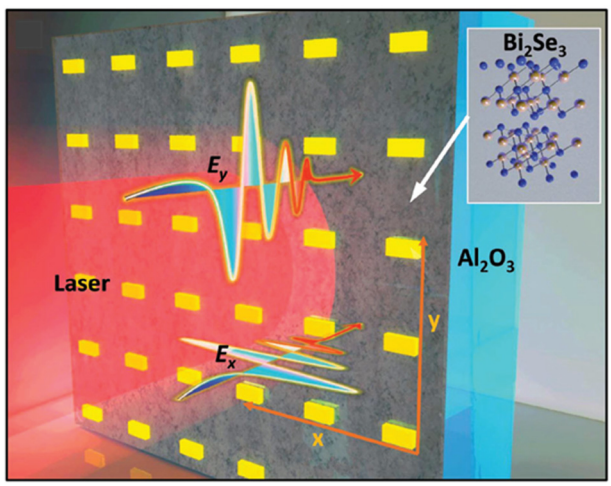


**FIG. 10.** A schematic diagram of the $Bi_2Se_3$-Au nanoantenna hybrid-structure sample on an $Al_2O_3$ substrate under laser irradiation.[58] Reproduced with permission from Miao *et al.*, Nanoscale **11**, 14598 (2019). Copyright 2019, Royal Society of Chemistry.

Various mechanisms have been proposed to create BICs. Decoupling is important for producing BICs. For periodic systems, BICs can be classified into two types: symmetry-protected BICs and parameter-tuned BICs.[63] Symmetry-protected BICs appear when the spatial symmetry of the model is different from the symmetry of the radiative wave propagating energy outward, and the coupling between the environment and modes is forbidden. Parameter-tuned BICs appear when radiation into all channels is completely suppressed by tuning the parameters of the system. BICs and quasi-BICs are generally used in applications such as lasing, sensing, and filtering. A BIC has an infinite quality factor in an ideal case with no radiation. It cannot be excited by waves coming from the far field, which makes it a great challenge to access from free space. A quasi-BIC breaks the symmetry of a structure with a finite quality factor. It can not only be excited by the outside field but can also radiate outward, which increases its range of application.[64]

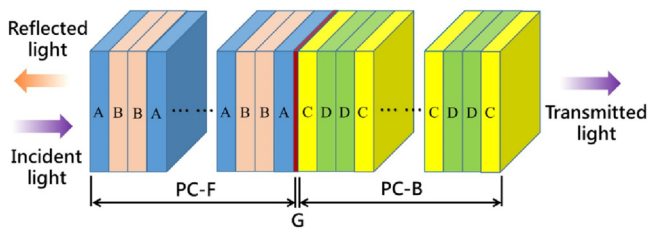


**FIG. 11.** Schematic diagram of the one-dimensional asymmetric topological photonic crystals with graphene.[59] Reproduced with permission from Lin *et al.*, Opt. Lett. **45**, 4369 (2020). Copyright 2020, Optical Society of America.

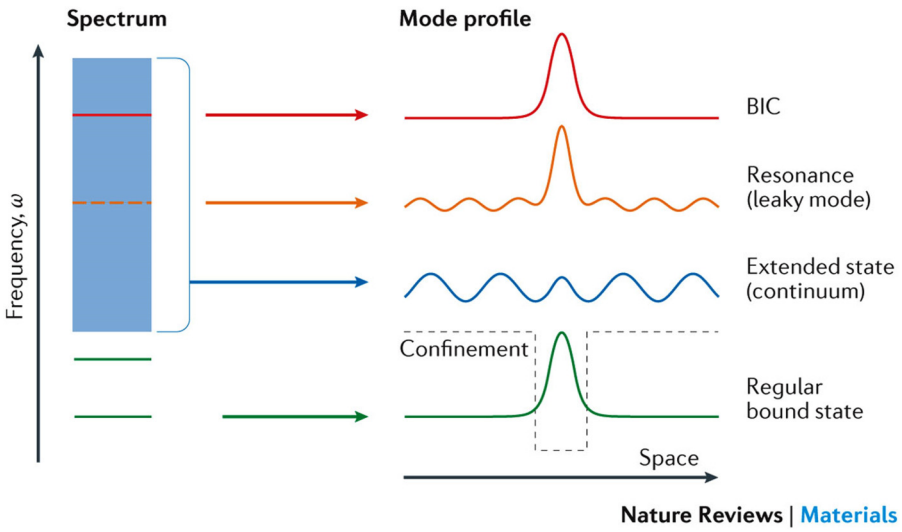


**FIG. 12.** Explanation of a BIC. Spectrum: the frequency spectrum consists of a continuum or several continua of spatially extended states (blue) and discrete levels of bound states (green) that carry no outgoing flux in an open system. Mode profile: Bound states in the continuum (BICs; red) are exceptional states that lie inside the continuum but remain localized without radiation. Leaky modes lie in the continuous spectrum typically couple to the extended waves and radiate, becoming leaky resonances with resonance frequency has imaginary part (orange). Spatially extended states (blue). Discrete levels of bound states (green).[60] Reproduced with permission from Hsu *et al.*, Nat. Rev. Mater. **1**, 16048 (2016). Copyright 2016, Springer Nature.

### *2. Examples of bound states in the continuum of an all-optical switch*

Quasi-BICs are always used to generate high Q resonances, which are important for enhancing light–matter interaction. In 2019, Liu *et al.* experimentally demonstrated a quasi-BIC with a record Q factor of 18 511 under normal excitation on an Si metasurface.[64] The result of the high Q resonances was sharp spectral resonance, which is very important for many applications such as optical switching,[65] imaging,[66] and filtering.[67]

In 2019, Karl *et al.*[68] explored a dielectric metasurface with its symmetry broken by removing a $230 \times 80\,\mathrm{nm}^2$ part from one corner of a $300 \times 300\,\mathrm{nm}^2$ unit structure, as shown in Fig. 13(a). The structures were arranged in a square array, and the lattice constant was 470 nm. A Fano resonance at 970 nm resulted from interaction between the in-plane ED and an out-of-plane MD and was observed in the reflectance spectrum. A spectral shift was achieved with a lower pump fluence ($89\,\mu\mathrm{J/cm}^2$) than previously achieved and with a short recovery time (2.5 ps), which could be applied to an optical switch. In 2020, Zhong *et al.*[69] proposed a configuration where a continuous graphene monolayer is placed between the dielectric grating and distributed Bragg reflector (DBR) layers, as Fig. 13(b) schematically depicts. This system effectively suppresses both the external leakage loss and intrinsic absorption loss. As the distance (hs) between the graphene and DBR increases, the resonance linewidth disappears and the Q factor increases quickly (up to 50 833), indicating the appearance of BICs. They further achieved high-performance switch manipulation by introducing a nonlinear dielectric. The switch was controlled from "OFF" to "ON" with a chemical potential of just 0.2 eV or a $5\,\mathrm{kW/cm}^2$ pump light, and the absorption contrast ratio reached 31 dB. In 2021, Han and Cai[70] used a slotted silicon disk array that showed a high

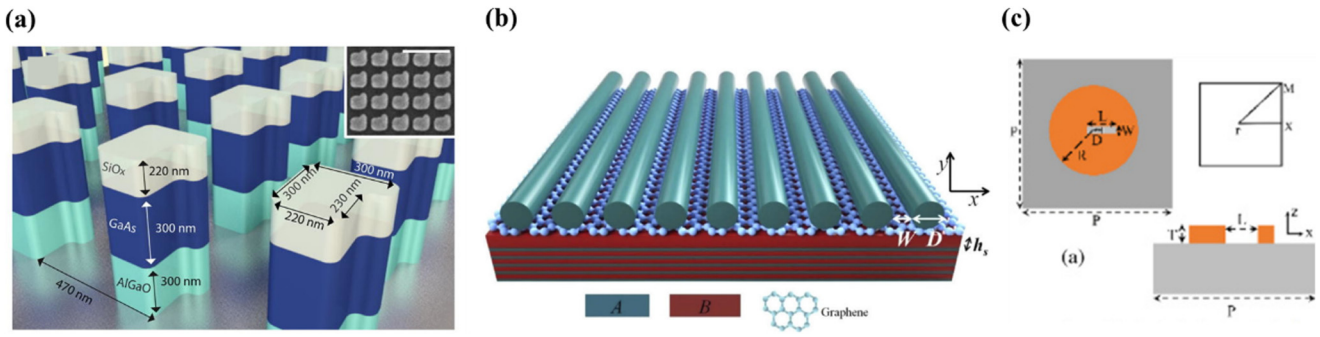


**FIG. 13.** (a) Illustration of the dielectric metasurface. The geometry of the three-layer symmetry broken structure with GaAs sandwiched by low index materials. The inset is the SEM image of the fabricated device.[68] Reproduced with permission from Karl *et al.*, Appl. Phys. Lett. **115**, 141103 (2019). Copyright 2019, AIP Publishing LLC. (b) Schematic representation of the structure of the ultrahigh Q graphene perfect absorber.[69] Reproduced with permission from Zhong *et al.*, Opt. Express **28**, 27294 (2020). Copyright 2020, Optical Society of America. (c) Schematic of the unit cell of slotted silicon disk array structure.[70] Reproduced with permission from Han *et al.*, Opt. Lett. **46**, 524 (2021). Copyright 2021, Optical Society of America.

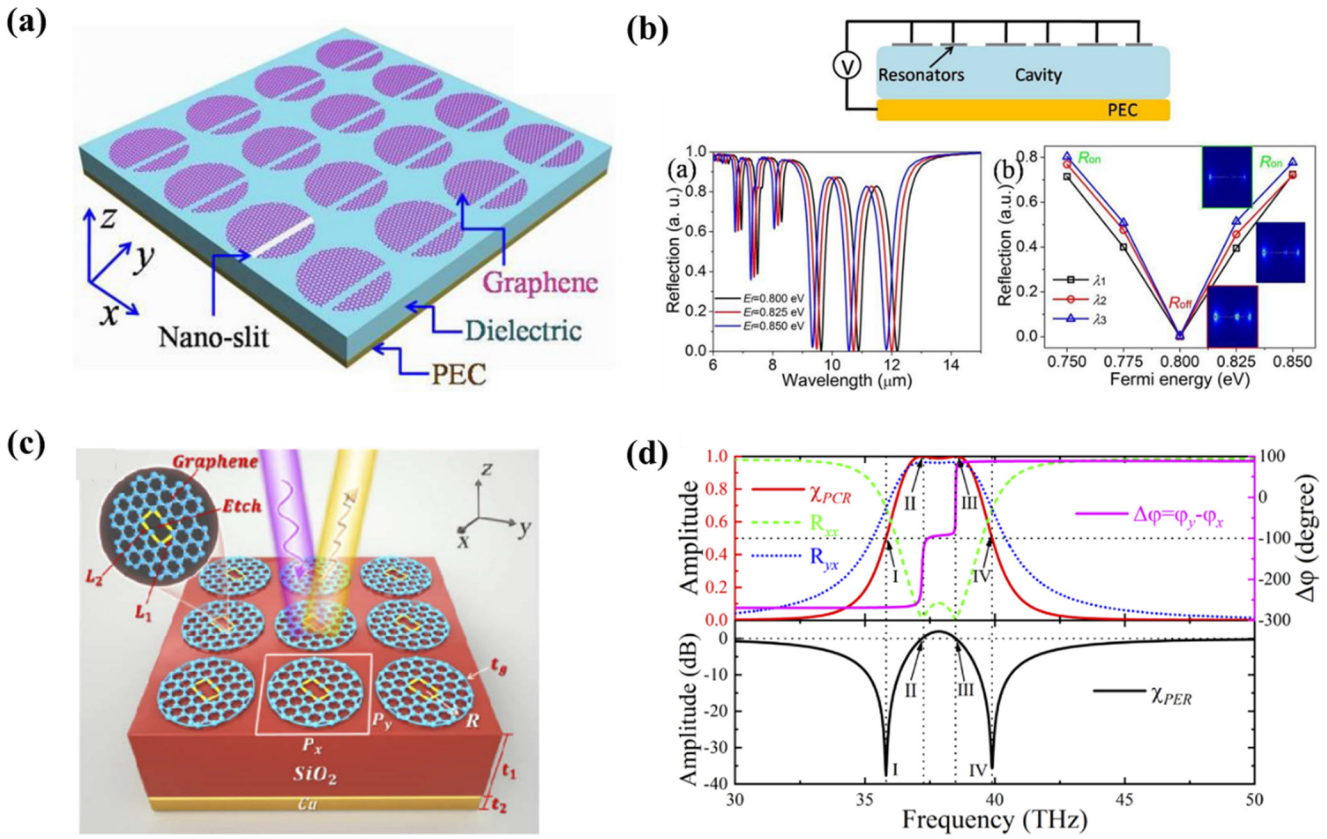


**FIG. 14.** (a) Schematic diagram of the GPPA. (b) Schematic of the electrical-adjusting plasmon switch by the absorber. Spectral reflection curves for the GPPA under certain Fermi energy for the graphene. Plotted reflection values for the reflection dips at l1–l3 as a function of Fermi energy, respectively. The corresponding electric field magnitude distributions are also shown as the inset. The blue and red colors indicate the weak and strong field distribution intensity, respectively.[72] Reproduced with permission from Liu *et al.*, Carbon **140**, 362 (2018). Copyright 2018, Elsevier Science &Technology Journals. (c) The schematic diagram of the proposed multi-functional polarization converter. (d) The amplitude of reflection coefficient components $R_{xx}$ and $R_{yx}$, the value of PCR $\chi_{PCR}$, the phase difference ($\Delta\varphi$) and the value of PER $\chi_{PER}$ under the incidence with x-polarization light. Points I, II, III, and IV are 35.81, 37.21, 38.49, and 39.89 THz, respectively.[73] Reproduced with permission from Zhang *et al.*, Opt. Express **29**, 70 (2021). Copyright 2021, Optical Society of America.

Q resonance based on BICs, which led to an all-optical self-switch. The unit cell and band structure are shown in Fig. 13(c). The BIC mode has no interaction with the external environment because all of its radiative channels are closed. The air slot plays an important role in the transition from the BIC mode to the quasi-BIC mode. This all-optical self-switch required a laser intensity of less than 1 kW/cm$^2$ to achieve a change in transmittance from 0 to more than 65%.

### D. Two-dimensional materials

Graphene, a flat sheet of carbon, is one of the best-known 2D materials and has an excellent linear dispersion relation. Its excellent electrical and optical properties, high carrier mobility, dynamic tunability, and high optical transparency give it potential for many devices such as optical switches, converters, sensors, and absorbers.[71]

The relatively low modulation efficiency and qualitative adjustment methods are still a problem. Liu *et al.* demonstrated a graphene plasmonic perfect absorber (GPPA) that not only provided perfect absorption in the multispectral range but also responded to artificially tunable absorption under external stimulation by the illumination polarization. They achieved a graphene plasmon switch with near-perfect modulation depth (99.9%) and ultrahigh relative modulation intensity (3590).[72] Figure 14(a) is the 3D schematic representation of the proposed GPPA, which is made of a periodic split graphene disk array and an opaque substrate sandwiched by a dielectric layer. An air nano-slit is introduced in the graphene disk at a certain distance away from the center. Figure 14(b) is the schematic representation of the proposed electrically controlled plasmonic switch. The Fermi energy levels of the graphene resonators are controlled through the applied voltage V.

In 2021, Zhang *et al.*[73] presented an efficient polarization conversion device with a hollow graphene metasurface. Figure 14(c)

shows the unit cell of the multi-functional polarization converter, which consists of a monolayer graphene disk with a hollow rectangle. The bottom of the graphene metasurface contains a silicon dioxide middle layer and a copper reflector substrate layer. This device achieves x-to-y cross-polarization conversion and linear-to-circular polarization conversion. Figure 14(d) shows the reflection coefficient components $R_{xx}$ and $R_{yx}$, the value of PCR $\chi_{PCR}$, and the phase difference $\Delta\varphi$ under x-polarized light.

## IV. CONCLUSION AND OUTLOOK

In conclusion, it is essential to introduce new physical principles to all-optical switches so they can achieve faster and lower energy consumption. All-optical switches are among the most important parts of integrated photonics. The traditional designs based on micro-ring resonators, SPPs, photonic crystals, and metamaterials can still be used, but the new physical concepts provide methods of designing ultrafast all-optical switches with ultralow energy consumption. PT symmetry, EPs, topological insulators, and bound states in a continuum have been very active research topics in photonics in recent years. On the one hand, people are looking for new physical phenomena, and on the other hand, they are also combining new physics with practical devices. There are still many performance indexes to be achieved to realize industrialization of the all-optical switch. New physical effects provide research ideas for the all-optical switch and broaden the design channel. This will likely lead to ultracompact, ultrafast, and high-capacity all-optical information processing in the future.

## AUTHORS' CONTRIBUTIONS

H.Q and X.W. contributed equally to this work.

## ACKNOWLEDGMENTS

This work was supported by the National Key Research and Development Program of China under Grant Nos. 2018YFB2200403 and 2018YFA0704404; the National Natural Science Foundation of China (NNSFC) under Grant Nos. 61775003, 11734001, 91950204, and 11527901; and Beijing Municipal Science and Technology Commission (No. Z191100007219001).

## REFERENCES

[1]G. Dong, W. Deng, J. Hou *et al.*, "Ultra-compact multi-channel all-optical switches with improved switching dynamic characteristics," Opt. Express **26**(20), 25630–25644 (2018).
[2]T. Morioka and M. Saruwatari, "Ultrafast all-optical switching utilizing the optical Kerr effect in polarization-maintaining single-mode fibers," IEEE J. Sel. Areas Commun. **6**(7), 1186–1198 (1988).
[3]M. Jinno and T. Matsumoto, "Ultrafast, low-power, and highly stable all-optical switching in an all polarization maintaining fiber Sagnac interferometer," IEEE Photonics Technol. Lett. **2**(5), 349–351 (1990).
[4]M. Asobe, H. Itoh, T. Miyazawa *et al.*, "Efficient and ultrafast all-optical switching using high delta-N, small core chalcogenide glass-fiber," Electron. Lett. **29**(22), 1966–1968 (1993).
[5]T. Morioka and M. Saruwatari, "All-optical ultrafast nonlinear switching utilizing the optical Kerr effect in optical fibers," Opt. Eng. **29**(3), 200–209 (1990).
[6]A. Hartsuiker, P. J. Harding, Y.-R. Nowicki-Bringuier *et al.*, "Kerr and free carrier ultrafast all-optical switching of GaAs/AlAs nanostructures near the three photon edge of GaAs," J. Appl. Phys. **104**(8), 083105 (2008).
[7]H. Lu, X. Liu, L. Wang *et al.*, "Ultrafast all-optical switching in nanoplasmonic waveguide with Kerr nonlinear resonator," Opt. Express **19**(4), 2910–2915 (2011).
[8]P. Colman, P. Lunnemann, Y. Yu *et al.*, "Ultrafast coherent dynamics of a photonic crystal all-optical switch," Phys. Rev. Lett. **117**(23), 233901 (2016).
[9]Q. M. Ngo, S. Kim, J. Lee *et al.*, "All-optical switches based on multiple cascaded resonators with reduced switching intensity-response time products," J. Lightwave Technol. **30**(22), 3525–3531 (2012).
[10]J. Covey, A. D. Finke, X. Xu *et al.*, "All-optical switching with 1-ps response time in a DDMEBT enabled silicon grating coupler/resonator hybrid device," Opt. Express **22**(20), 24530–24544 (2014).
[11]P. Ma, H. Jackel, G. L. Bona *et al.*, "Ultrafast, compact, and energy efficient all-optical switches based on a saturable absorbing cavity," IEEE J. Quantum Electron. **50**(12), 1019–1028 (2014).
[12]M. Ono, M. Hata, M. Tsunekawa *et al.*, "Ultrafast and energy-efficient all-optical switching with graphene-loaded deep-subwavelength plasmonic waveguides," Nat. Photonics **14**(1), 37 (2020).
[13]V. Rutckaia and J. Schilling, "Ultrafast low-energy all-optical switching," Nat. Photonics **14**(1), 4–6 (2020).
[14]T. F. Khalkhali, B. Rezaei, A. S. Vala *et al.*, "Design of high-Q polystyrene nonlinear cavity for ultrafast all-optical switching in mid-infrared photonic crystal slabs with cavity-waveguide structure," Opt. Commun. **326**(9), 43–47 (2014).
[15]Z. M. Meng, Y. H. Hu, C. Wang *et al.*, "Design of high-Q silicon-polymer hybrid photonic crystal nanobeam microcavities for low-power and ultrafast all-optical switching," Photonics Nanostruct. Fundam. Appl. **12**(1), 83–92 (2014).
[16]E. Dremetsika, B. Dlubak, S.-P. Gorza *et al.*, "Measuring the nonlinear refractive index of graphene using the optical Kerr effect method," Opt. Lett. **41**(14), 3281–3284 (2016).
[17]H. Rahimi, "Kerr-type nonlinear response of a graphene-coated quasiperiodic structure composed of silicon dioxide and polystyrene layers in the THz region," Phys. B: Condens. Matter **550**, 274–279 (2018).
[18]Y. Zhang, J. Wu, Y. Yang *et al.*, "Enhanced Kerr nonlinearity and nonlinear figure of merit in silicon nanowires integrated with 2D graphene oxide films," ACS Appl. Mater. Interfaces **12**(29), 33094–33103 (2020).
[19]S. Bugaychuk, A. Iljin, O. Lytvynenko *et al.*, "Enhanced nonlinear optical effect in hybrid liquid crystal cells based on photonic crystal," Nanoscale Res. Lett. **12**, 499 (2017).
[20]K. Bae, J. Zhu, C. Wolenski *et al.*, "Indium tin oxide nanoparticle-coated silica microsphere with large optical nonlinearity and high quality factor," ACS Photonics **7**(11), 3042–3048 (2020).
[21]M. Esmaeili, E. Koushki, and H. Mousavi, "Nonlinear optical re-orientation and photoacoustic properties of indium tin oxide nanoparticles," Phys. E **120**, 114063 (2020).
[22]K. P. Kelley, E. L. Runnerstrom, E. Sachet *et al.*, "Multiple epsilon-near-zero resonances in multilayered cadmium oxide: Designing metamaterial-like optical properties in monolithic materials," ACS Photonics **6**(5), 1139–1145 (2019).
[23]L. Zhao and H. Xie, "A novel optical e-near-zero material realized by multi-layered Ag/SiC film structures," Optik **183**, 513–522 (2019).
[24]M. T. Hill, H. J. S. Dorren, T. de Vries *et al.*, "A fast low-power optical memory based on coupled micro-ring lasers," Nature **432**(7014), 206–209 (2004).
[25]D. O'Carroll, I. Lieberwirth, and G. Redmond, "Microcavity effects and optically pumped lasing in single conjugated polymer nanowires," Nat. Nanotechnol. **2**(3), 180–184 (2007).
[26]M. Forst, J. Niehusmann, T. Plotzing *et al.*, "High-speed all-optical switching in ion-implanted silicon-on-insulator microring resonators," Opt. Lett. **32**(14), 2046–2048 (2007).
[27]M. Waldow, T. Plotzing, M. Gottheil *et al.*, "25ps all-optical switching in oxygen implanted silicon-on-insulator microring resonator," Opt. Express **16**(11), 7693–7702 (2008).

[28]J. S. Pelc, K. Rivoire, S. Vo *et al.*, "Picosecond all-optical switching in hydrogenated amorphous silicon microring resonators," Opt. Express **22**(4), 3797–3810 (2014).
[29]J. J. Xiao, K. Yakubo, and K. W. Yu, "Optical switching in graded plasmonic waveguides," Appl. Phys. Lett. **88**(24), 241111 (2006).
[30]G. A. Wurtz and A. V. Zayats, "Nonlinear surface plasmon polaritonic crystals," Laser Photonics Rev. **2**(3), 125–135 (2008).
[31]Z. Zhang, J. Yang, X. He *et al.*, "All-optical multi-channel switching at telecommunication wavelengths based on tunable plasmon-induced transparency," Opt. Commun. **425**, 196–203 (2018).
[32]A. Karabchevsky, A. Hazan, and A. Dubavik, "All-optical polarization-controlled nanosensor switch based on guided-wave surface plasmon resonance via molecular overtone excitations in the near-infrared," Adv. Opt. Mater. **8**(19), 2000769 (2020).
[33]Y. A. Vlasov, M. O'Boyle, H. F. Hamann *et al.*, "Active control of slow light on a chip with photonic crystal waveguides," Nature **438**(7064), 65–69 (2005).
[34]A. Sipahigil, R. E. Evans, D. D. Sukachev *et al.*, "An integrated diamond nanophotonics platform for quantum-optical networks," Science **354**(6314), 847–850 (2016).
[35]Z. Chai, X. Hu, F. Wang *et al.*, "Ultrafast on-chip remotely-triggered all-optical switching based on epsilon-near-zero nanocomposites," Laser Photonics Rev. **11**(5), 1700042 (2017).
[36]M. Takiguchi, N. Takemura, K. Tateno *et al.*, "All-optical InAsP/InP nanowire switches integrated in a Si photonic crystal," ACS Photonics **7**(4), 1016–1021 (2020).
[37]D. R. Smith, J. B. Pendry, and M. C. K. Wiltshire, "Metamaterials and negative refractive index," Science **305**(5685), 788–792 (2004).
[38]C. L. Holloway, E. F. Kuester, J. A. Gordon *et al.*, "An overview of the theory and applications of metasurfaces: The two-dimensional equivalents of metamaterials," IEEE Antennas Propag. Mag. **54**(2), 10–35 (2012).
[39]M. Shoaei, M. K. Moravvej-Farshi, and L. Yousefi, "All-optical switching of nonlinear hyperbolic metamaterials in visible and near-infrared regions," J. Opt. Soc. Am. B: Opt. Phys. **32**(11), 2358–2365 (2015).
[40]Z. T. Xie, J. Y. Wu, H. Y. Fu *et al.*, "Tunable electro- and all-optical switch based on epsilon-near-zero metasurface," IEEE Photonics J. **12**(4), 4501510 (2020).
[41]P. Sethi and S. Roy, "All-optical ultrafast switching in 2×2 silicon microring resonators and its application to reconfigurable DEMUX/MUX and reversible logic gates," J. Lightwave Technol. **32**(12), 2173–2180 (2014).
[42]A. Granpayeh, H. Habibiyan, and P. Parvin, "Photonic crystal directional coupler for all-optical switching, tunable multi/demultiplexing and beam splitting applications," J. Mod. Opt. **66**(4), 359–366 (2019).
[43]S. Rebhi and M. Najjar, "Hourglass nonlinear photonic crystal cavity for ultrafast all-optical switching," Optik **180**, 858–865 (2019).
[44]S. Khani, M. Danaie, and P. Rezaei, "Compact and low-power all-optical surface plasmon switches with isolated pump and data waveguides and a rectangular cavity containing nano-silver strips," Superlattices Microstruct. **141**, 106481 (2020).
[45]C. M. Bender and S. Boettcher, "Real spectra in non-Hermitian Hamiltonians having PT symmetry," Phys. Rev. Lett. **80**(24), 5243–5246 (1998).
[46]R. El-Ganainy, K. G. Makris, D. N. Christodoulides *et al.*, "Theory of coupled optical PT-symmetric structures," Opt. Lett. **32**(17), 2632–2634 (2007).
[47]K. G. Makris, R. El-Ganainy, D. N. Christodoulides *et al.*, "Beam dynamics in PT symmetric optical lattices," Phys. Rev. Lett. **100**(10), 103094 (2008).
[48]Z. Zhang, Y. Zhang, J. Sheng *et al.*, "Observation of parity-time symmetry in optically induced atomic lattices," Phys. Rev. Lett. **117**(12), 123601 (2016).
[49]M.-A. Miri and A. Alù, "Exceptional points in optics and photonics," Science **363**(42), eaar7709 (2019).
[50]C. E. Ruter, K. G. Makris, R. El-Ganainy *et al.*, "Observation of parity-time symmetry in optics," Nat. Phys. **6**(3), 192–195 (2010).
[51]S. K. Ozdemir, S. Rotter, F. Nori *et al.*, "Parity-time symmetry and exceptional points in photonics," Nat. Mater. **18**(8), 783–798 (2019).
[52]A. Guo, G. J. Salamo, D. Duchesne *et al.*, "Observation of PT-symmetry breaking in complex optical potentials," Phys. Rev. Lett. **103**(9), 093902 (2009).
[53]J. Doppler, A. A. Mailybaev, J. Bohm *et al.*, "Dynamically encircling an exceptional point for asymmetric mode switching," Nature **537**(7618), 76–79 (2016).
[54]A. U. Hassan, B. Zhen, M. Soljacic *et al.*, "Dynamically encircling exceptional points: Exact evolution and polarization state conversion," Phys. Rev. Lett. **118**(9), 093002 (2017).
[55]A. Laha, D. Beniwal, S. Dey *et al.*, "Third-order exceptional point and successive switching among three states in an optical microcavity," Phys. Rev. A **101**(6), 063829 (2020).
[56]J. E. Moore, "The birth of topological insulators," Nature **464**(7286), 194–198 (2010).
[57]Y. Wu, X. Hu, and Q. Gong, "Reconfigurable topological states in valley photonic crystals," Phys. Rev. Mater. **2**(12), 122201 (2018).
[58]R. Miao, Y. Hu, H. Ouyang *et al.*, "A polarized nonlinear optical response in a topological insulator $Bi_2Se_3$-Au nanoantenna hybrid-structure for all-optical switching," Nanoscale **11**(31), 14598–14606 (2019).
[59]Y. C. Lin, S. H. Chou, and W. J. Hsueh, "Tunable light absorption of graphene using topological interface states," Opt. Lett. **45**(16), 4369–4372 (2020).
[60]C. W. Hsu, B. Zhen, A. D. Stone *et al.*, "Bound states in the continuum," Nat. Rev. Mater. **1**(9), 16048 (2016).
[61]L. Fonda, "Bound states embedded in the continuum and the formal theory of scattering," Ann. Phys. **22**(1), 123–132 (1963).
[62]H. Friedrich and D. Wintgen, "Physical realization of bound-states in the continuum," Phys. Rev. A **31**(6), 3964–3966 (1985).
[63]Q. Song, J. Hu, S. Dai *et al.*, "Coexistence of a new type of bound state in the continuum and a lasing threshold mode induced by PT symmetry," Sci. Adv. **6**(34), eabc1160 (2020).
[64]Z. Liu, Y. Xu, Y. Lin *et al.*, "High-Q quasibound states in the continuum for nonlinear metasurfaces," Phys. Rev. Lett. **123**(25), 253901 (2019).
[65]A. E. Miroshnichenko, S. Flach, and Y. S. Kivshar, "Fano resonances in nanoscale structures," Rev. Mod. Phys. **82**(3), 2257–2298 (2010).
[66]A. Tittl, A. Leitis, M. Liu *et al.*, "Imaging-based molecular barcoding with pixelated dielectric metasurfaces," Science **360**(6393), 1105 (2018).
[67]Y. Shuai, D. Zhao, Z. Tian *et al.*, "Double-layer fano resonance photonic crystal filters," Opt. Express **21**(21), 24582–24589 (2013).
[68]N. Karl, P. P. Vabishchevich, S. Liu *et al.*, "All-optical tuning of symmetry protected quasi bound states in the continuum," Appl. Phys. Lett. **115**(14), 141103 (2019).
[69]H. Zhong, Z. Liu, X. Liu *et al.*, "Ultra-high quality graphene perfect absorbers for high performance switching manipulation," Opt. Express **28**(25), 37294–37306 (2020).
[70]Z. Han and Y. Cai, "All-optical self-switching with ultralow incident laser intensity assisted by a bound state in the continuum," Opt. Lett. **46**(3), 524–527 (2021).
[71]Z. Chai, X. Hu, F. Wang *et al.*, "Ultrafast all-optical switching," Adv. Opt. Mater. **5**(7), 1600665 (2017).
[72]X. Liu, G. Liu, P. Tang *et al.*, "Quantitatively optical and electrical-adjusting high-performance switch by graphene plasmonic perfect absorbers," Carbon **140**, 362–367 (2018).
[73]H. Zhang, Y. Liu, Z. Liu *et al.*, "Multi-functional polarization conversion manipulation via graphene-based metasurface reflectors," Opt. Express **29**(1), 70–81 (2021).